

Attenuation effect of artificial cavity on air-blast waves in an intelligent defense layer

Zhi-liang Wang ^{a,b,*}, J.G. Wang ^c, Yong-chi Li ^a, C.F. Leung ^d

^a Department of Mechanics and Mechanical Engineering, University of Science and Technology of China, Anhui province, Hefei 230027, China

^b College of Civil Engineering, Hefei University of Technology, Anhui province, Hefei 230027, China

^c Centre for Protective Technology, National University of Singapore, 10 Kent Ridge Crescent, Singapore 119260, Singapore

^d Department of Civil Engineering, National University of Singapore, 10 Kent Ridge Crescent, Singapore 119260, Singapore

Received 5 April 2005; received in revised form 24 January 2006; accepted 7 February 2006

Available online 30 March 2006

Abstract

Civil defense shelters are often constructed beneath the ground to provide protection against blast loads. Concrete is widely used as the material for the defense layer of the shelters and artificial cavities are often embedded in the concrete to ensure adequate attenuation of the air-blast waves. This paper employs the Johnson–Holmquist–Concrete model, an elastoplastic damage model, to investigate the effects of artificial cavities on the attenuation of air-blast waves in the concrete defense layer. The results reveal that the peak axial stress beneath a cavity is largely reduced and the elastoplastic and damage properties of the concrete play significant roles on the wave attenuation. Two empirical formulae are then proposed to relate the decay factor of peak axial stress to the dimensions and relative positions of rectangular and circular cavities. Finally, the effects of multiple cavities on the attenuation of air-blast waves are investigated.

© 2006 Elsevier Ltd. All rights reserved.

Keywords: Defense layer; Air-blast waves; Cavity shape; Cavity dimensions; Decay factor; Empirical formula; Multiple cavities

1. Introduction

The propagation and diffraction of air-blast induced stress-waves are important considerations in anti-blast design. The development of modern military technology greatly enhances the destructive power and hit rate of new weapons, thus posing great challenges to defense engineering nowadays. Civil defense shelters are widely constructed beneath the ground to provide protection against blast loads [1,2]. Blast waves due to far-field detonation evolve into propagation of stress-waves in underground media. Such waves will diffract when hitting obstacles, such as cavity, crevice or other media. The wave stress intensity may be greatly reduced beneath these obstacles. This

reduction of stress from the peak value is often termed as attenuation or insulation of stress-waves [3,4].

The diffraction and attenuation of stress-waves are important aspects in the design of civil defense shelters [1,4–6]. To design a civil defense structure, the reduction of stress-waves needs to be examined. In addition, new stress-wave migrating and weakening systems are expected [7]. In this paper, investigations will be focused on the reduction of stress-waves through an intelligent defense layer embedded with artificial cavities.

Fig. 1(a) shows that an intelligent defense layer usually consists of three layers [5,8]: an earth cover layer, a protection layer and a support layer. The protection layer often has two sub-layers: a projectile shelter layer and a stress distribution layer. The projectile shelter layer provides resistance against penetration, and several design schemes on the topic have been proposed so far [8–10]. The stress distribution layer is employed to redistribute

* Corresponding author. Fax: +86 551 3606459.

E-mail address: zliangw@ustc.edu.cn (Z.-l. Wang).

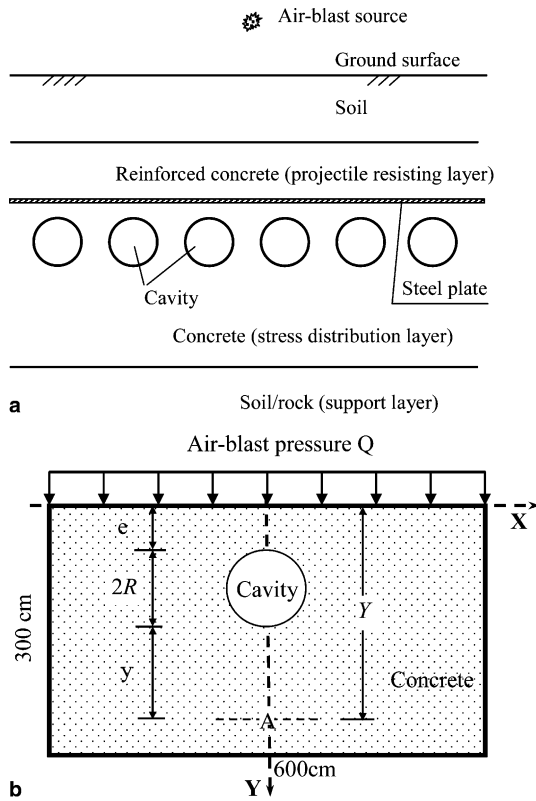


Fig. 1. Typical defense shelter and simulation of stress distribution layer. (a) Typical defense shelter. (b) Computational domain for stress distribution layer.

or diffuse the blast loading. Till to date, relatively few studies have been carried out to examine the stress redistribution in this layer. For example, artificial cavities are constructed in the stress distribution layer to dissipate the energy of stress-waves. However, the function and design methodology of these cavities have not been thoroughly examined so far [11–16]. Furthermore, concrete is commonly employed as the material of these intelligent defense layers in protective facilities. Upon blast loading, the concrete medium usually experiences elastoplastic deformation and even damage and this may affect the attenuation of the stress-waves. However, the effects of elastoplastic and damage properties of concrete on the attenuation of stress-waves are not well understood. In addition, very little is known on the screen effect of cavities.

In this paper, numerical analyses have been carried out to investigate the effect of an embedded cavity on the attenuation of stress-waves in concrete medium using the Johnson–Holmquist–Concrete (J–H–C) model [17,18]. In particular, the influence of cavity on the decay factors of peak axial stress, σ_y , is examined in detail using rectangular and circular shaped cavities. Based on the numerical results, empirical formulae are proposed to relate the decay factor for peak stress to the cavity parameters. Finally, the effects of multiple cavities are studied and compared with that of single cavity.

2. Computational problem for a typical intelligent layer

2.1. Definition of decay factor

To evaluate the attenuation extent of a stress-wave due to a cavity in an intelligent defense layer, a dimensionless variable, ‘decay factor’ DF, is defined as follows:

$$DF = \frac{\sigma_0 - \sigma}{\sigma_0} \quad (1)$$

where σ_0 denotes the peak value of stress component, such as σ_x , σ_y , and hydrostatic pressure P at a specified position without cavity in the defense layer, and σ is the peak value of the same component at the same position with a cavity in the defense layer. Eq. (1) reveals that a larger DF would imply a superior attenuation effect.

2.2. Computational domain with circular cavity

A typical concrete defense layer embedded with a circular cavity is shown in Fig. 1(b). This is a two-dimensional model whose computational domain is taken as 600 cm × 300 cm (width × height). The upper apex of the cavity is at a depth e beneath the surface and the circular cavity has a radius R . Thus, the coordinates of the center is $(0, e + R)$. Other dimensions are labeled in Fig. 1(b). Introducing the term relative distance y as the distance between point A and the lower apex of the cavity, the dimension Y follows the following relationship:

$$Y = y + 2R + e \quad (2)$$

Only half of the domain is selected in the computations owing to symmetry. As an example, the right half domain shown in Fig. 1(b) has the following boundary conditions: pressure boundary on the top, transmission boundaries (no reflection) on the right and lower sides, and symmetric boundary on the left side.

2.3. Air-blast loading

A spherical front of blast waves are reported to be developed during an explosion in the air [19,20]. The initial high pressure decreases as the wave propagates through the air. As the blast wave front is much larger than the dimensions of the defense layer, the air-blast loading or overpressure can be assumed to be uniform over the entire upper surface of the defense layer. In addition, because the overpressure decays exponentially, it can be approximated by an equivalent triangular pressure pulse as shown in Fig. 2 [21,22]. The intensity and duration of this overpressure depend on the explosive charge weight and the stand-off distance which usually follows the cubic laws [1,21–23]. In the present study, the peak value Q_{\max} is taken as 120 MPa and occurs at time $t_{\max} = 0 \mu\text{s}$ (micro second). This peak overpressure then decreases linearly to zero at time $t_c = 100.0 \mu\text{s}$. Such an overpressure corresponds to the charge weight

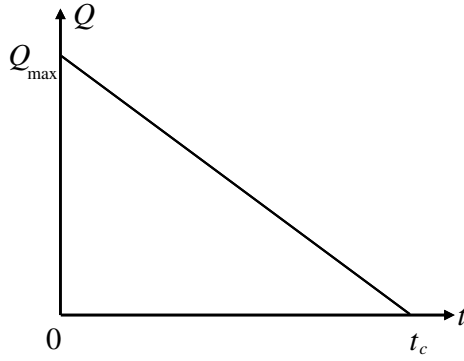


Fig. 2. Triangular impulse loading for explosion.

of 885 kg (TNT explosive) and stand-off distance of 5 m in the air.

2.4. Numerical tools for analysis

The LS-DYNA software from the Livermore Software Technology Corporation is used in the present study to carry out all computations. This software can handle either two- or three-dimensional problems for high-speed impact and explosion [24,25].

3. Constitutive law of concrete medium

Concrete is typically nonhomogeneous in composition and may possess flaws, such as cracks and voids. Strictly speaking, the linear-elastic model (L-E model) can only describe its initial deformation [17,26]. Under air-blast loading, the flaws may cause elastoplastic and damage deformations in the concrete medium. The elastoplastic damage process is irreversible and dissipates the stress-wave energy. This paper adopts the J–H–C model [17,18,23], which has been specifically developed for concrete subject to high pressures, large strains, and high strain rates. As seen from Fig. 3, this model has three components: strength criterion with strain rate effect, damage evolution with plastic deformation, and nonlinear hydrostatic compression.

3.1. Strength with strain rate effect

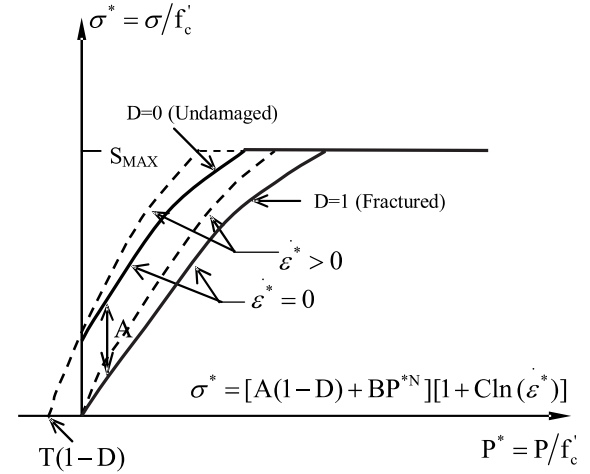
If the equivalent stress σ is normalized by the quasi-static uniaxial compressive strength f'_c , a normalized equivalent stress σ^* is defined as

$$\sigma^* = \frac{\sigma}{f'_c} \quad (3)$$

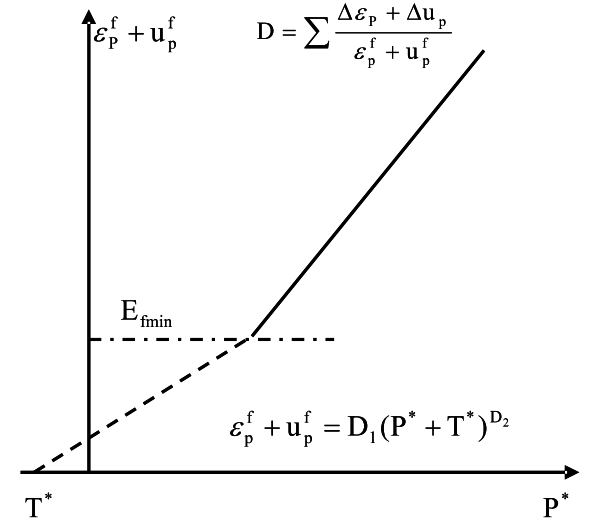
σ^* is a function of pressure P , strain rate $\dot{\epsilon}$ and damage parameter D

$$\sigma^* = [A(1-D) + B \cdot P^{*N}][1 + C \cdot \ln(\dot{\epsilon}^*)] \quad (4)$$

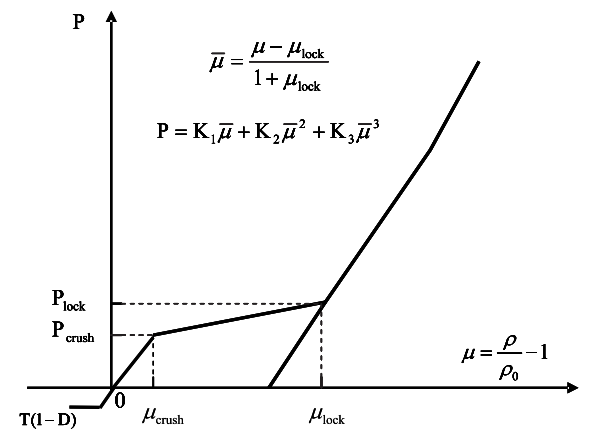
where $P^* = \frac{P}{f'_c}$ denotes the normalized pressure, and $\dot{\epsilon}^* = \frac{\dot{\epsilon}}{\dot{\epsilon}_0}$ is the dimensionless strain rate. In addition, A is the normalized cohesion, B is the coefficient for the normalized



a



b



c

Fig. 3. Elastoplastic damage constitutive model of concrete medium. (a) Constitutive model. (b) Damage. (c) Hydrostatic compression pressure versus volumetric strain.

pressure hardening, C denotes the coefficient of strain rate, and N is an exponent for the pressure hardening. The damage parameter D will be examined next.

3.2. Damage parameter

In the present model, the damage parameter D is defined by the accumulation of both generalized deviatoric plastic strain ε_p and plastic volumetric strain μ_p . It is expressed as

$$D = \sum \frac{\Delta \varepsilon_p + \Delta \mu_p}{D_1(P^* + T^*)^{D_2}} \quad (5)$$

where Δ denotes the increment and \sum denotes their summation along the deformation history; $T^* = \frac{T}{f'_c}$ is the normalized hydrostatic pressure; and D_1 and D_2 are the material constants. It is noted that the damage parameter D varies within the range of 0–1. When $D = 0$, no damage is observed; and when $D = 1$, the concrete is completely damaged and cannot resist any shear stress.

3.3. Hydrostatic compression

Since concrete is formed by granular materials, its mechanical behavior depends on the hydrostatic pressure. The hydrostatic pressure–volume relationship is presented in Fig. 3(c). The compressive deformation of concrete experiences the following three stages:

- (a) Elastic stage ($0 \leq \mu \leq \mu_{\text{crush}}$)

$$P = K_1 \mu, \quad \mu = \frac{\rho}{\rho_0}, \quad K_1 = \frac{P_{\text{crush}}}{\mu_{\text{crush}}} \quad (6)$$

where ρ , ρ_0 are the current and initial densities, respectively; μ_{crush} is the crushing volumetric strain; P_{crush} the crushing pressure; and K_1 the bulk modulus.

- (b) Transition stage ($\mu_{\text{crush}} < \mu \leq \mu_{\text{lock}}$) The μ_{lock} is the locking volumetric strain. The bubbles in concrete are broken in this stage, causing damage of the concrete structure, but the integrity of concrete medium is still maintained.

- (c) Compact stage ($\mu > \mu_{\text{lock}}$) The concrete is now fully dense material without air and voids. The pressure P for this fully dense material is formulated as

$$P = K_1 \bar{\mu} + K_2 \bar{\mu}^2 + K_3 \bar{\mu}^3 \quad (7)$$

where K_1 , K_2 , K_3 are material constants. The modified volumetric strain $\bar{\mu}$ is defined as:

$$\bar{\mu} = \frac{\mu - \mu_{\text{lock}}}{1 + \mu_{\text{lock}}} \quad (8)$$

4. Numerical investigations

4.1. Circular cavity

4.1.1. Effect of cavity radius R

Five radii are chosen in the computations: 0.0, 0.15, 0.30, 0.45 and 0.60 m, respectively. The parameter e is fixed as 0.30 m. The model parameters for concrete are given in

Table 1
Model parameters for concrete^a

<i>Density</i>	
ρ_0 (kg/m ³)	2440
<i>Elastic constants</i>	
G (GPa)	14.86
V	0.20
K_1 (GPa)	85.0
<i>Damage constants</i>	
D_1	0.04
D_2	1.0
E_{fmin}^b	0.01
<i>Pressure constants</i>	
P_{crush} (GPa)	0.016
μ_{crush}	0.001
P_{lock} (GPa)	0.80
μ_{lock}	0.10
K_1 (GPa)	85.0
K_2 (GPa)	−171.0
K_3 (GPa)	208.0
T (GPa)	0.004
<i>Strength constants</i>	
A	0.79
B	1.60
C	0.007
N	0.61
f'_c (GPa)	0.048
S_{MAX}	7.0
$\dot{\varepsilon}_0$ (s ^{−1})	10 ^{−6}

^a Unconfined compressive strength of concrete = 48 MPa.

^b E_{fmin} is the amount of plastic strain before fracture.

Table 1. For comparisons, the computations are also carried out for the L-E model. The variations of peak axial stress σ_y with relative distance y (refer to the definition shown in Fig. 1) are shown in Fig. 4(a) for the J–H–C model and Fig. 4(b) for the L-E model. In both cases, the peak σ_y decreases with increase in radius R for a specified position y . On the other hand, the peak σ_y increases with relative distance y for a nonzero R . Comparing the magnitudes of the peak axial stress σ_y in Fig. 4(a) and (b), it can be seen that the elastoplastic properties of concrete plays a crucial role on the magnitude of peak axial stress. For instance, when $R = 0.30$ m and $y = 0.60$ m, the peak σ_y is 51.8 MPa for the L-E model and only 25.2 MPa for the J–H–C model. The change of decay factor DF with R is shown in Fig. 5 for the J–H–C model. This figure shows that the DF increases with R but reduces with increasing y .

The hydrostatic pressure contours are shown in Fig. 6(a) and the damage contours are shown in Fig. 6(b). These figures show that the stress-wave is disrupted due to the presence of cavity. A stress concentration is observed in the left and right sides of the cavity, with a maximum value of almost 12 MPa. A zero-stress region is noted in the adjacent domain beneath the cavity. The peak σ_y beneath the cavity is evidently lower. Referring to Fig. 6 (b), the damage zone is mainly located at the upper surface of the problem domain. Therefore, the

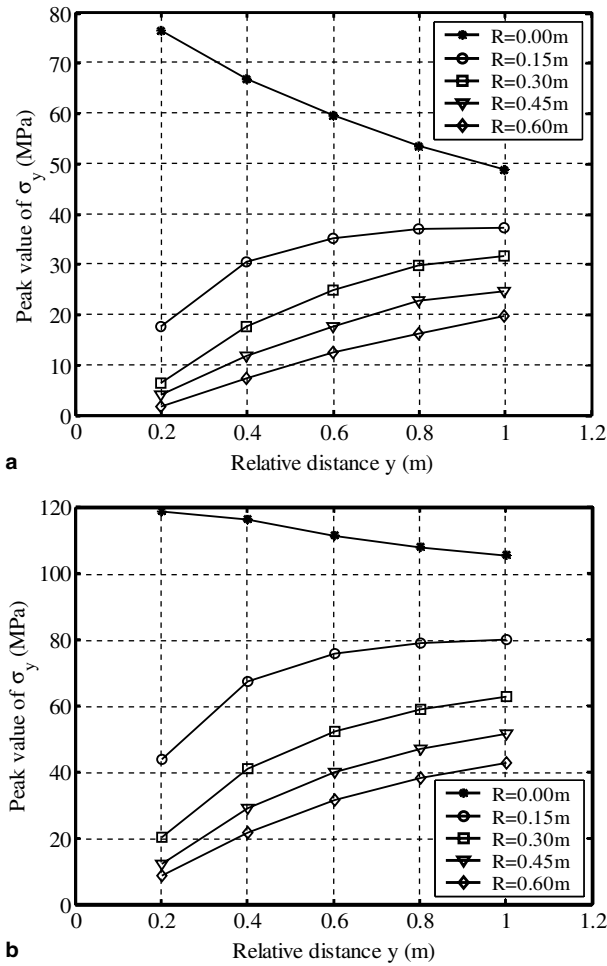


Fig. 4. Effect of different radii R of circular cavity on peak axial stress σ_y . (a) J-H-C model. (b) L-E model.

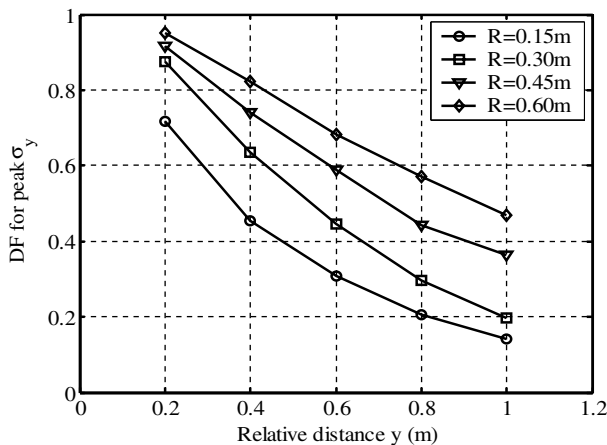


Fig. 5. Variation of decay factors for the peak σ_y with different radii R of cavity for JHC model.

air-blast loading may cause spalling at the roof of the cavity. Special protection is necessary when the peak value of blast loading is much larger.

4.1.2. Effect of cavity position e

The effect of the cavity position e on the attenuation of stress waves is shown in Fig. 7. When R is fixed, the decay factors DF are practically identical for all e values. This phenomenon can be also observed from the time-hydrostatic pressure curves at $y = 0.5\text{ m}$ shown in Fig. 8. The peak value of hydrostatic pressure does not vary much for all e values. It should be noted that the above results are obtained when the cavity has not collapsed.

4.1.3. Empirical formula for decay factor

Based on the above numerical results, it is established that DF is essentially a function of R and y :

$$DF = f(R, y) \quad (9)$$

where the relative distance $y = Y - 2R - e$.

In order to determine the particular form of Eq. (9), one value of e (0.30 m), four values of R (0.15, 0.30, 0.45 and 0.60 m) and five values of y (0.2, 0.4, 0.6, 0.8 and 1.0 m) are chosen from Fig. 5. Through a curve fitting regression analysis, the DF for the peak σ_y at a specified point on the Y -axis is approximately expressed as follows:

$$DF = 1 - \exp\left(-\frac{R}{y}\right) \quad (10)$$

This formula shows that DF increases with R and decreases with increasing y . When $\frac{y}{R}$ approaches to zero, the DF is almost equal to unity. Fig. 9 shows the comparison of numerical results with the predictions from the above empirical formula. It is clear that this empirical formula gives a reasonable good fitting to the numerical results. Therefore, Eq. (10) can be used to estimate the radius R of a circular cavity if the expected DF (at a relative distance y) and position e are known. On the other hand, when DF and R are given, the relative distance y can be also determined from Eq. (10).

4.2. Rectangular cavity

Rectangular cavities are also often built in the defense layer. The effect of a rectangular cavity on the attenuation of stress-waves will be numerically investigated in this section. The embedded cavity has the dimensions of $2l$ in length and h in width. Other dimensions are indicated in Fig. 10. The dimension Y has the following relationship:

$$Y = y + e + h \quad (11)$$

In the computations, the constitutive model of concrete and boundary conditions are the same as those for the circular cavity case. A half domain is also considered here owing to symmetry.

4.2.1. Effect of cavity length l

Five lengths are taken in the computations: 0.0, 0.3, 0.6, 0.9 and 1.2 m. Other geometrical parameters are fixed as

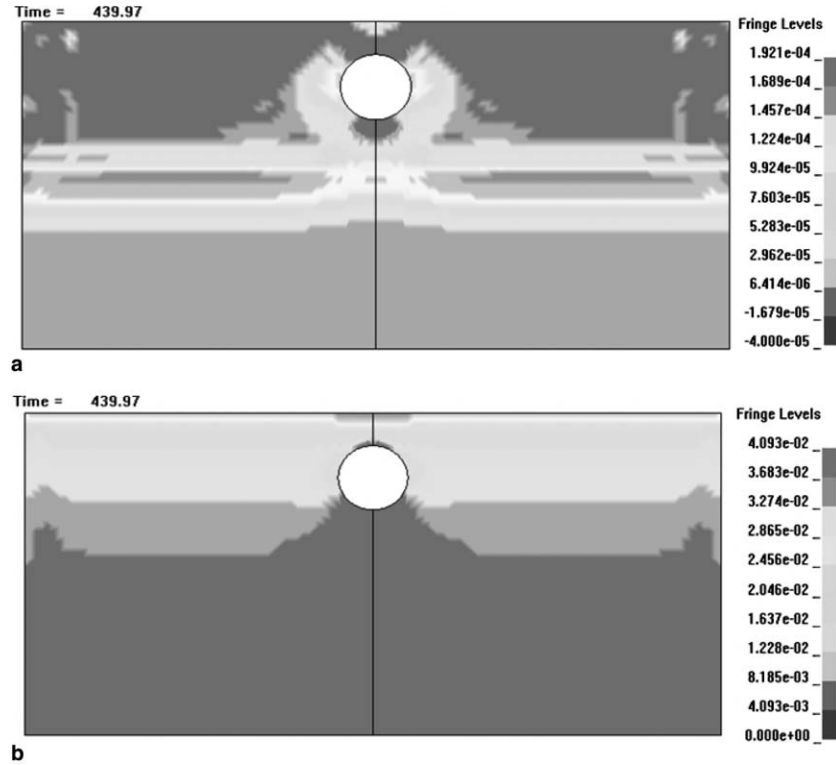


Fig. 6. Contours of pressure and damage for $R = 0.30$ m cavity at $t = 440 \mu\text{s}$ when subject to air-blast wave. (a) Pressure (unit: Mbar, 1 Mbar = 10^5 MPa). (b) Damage.

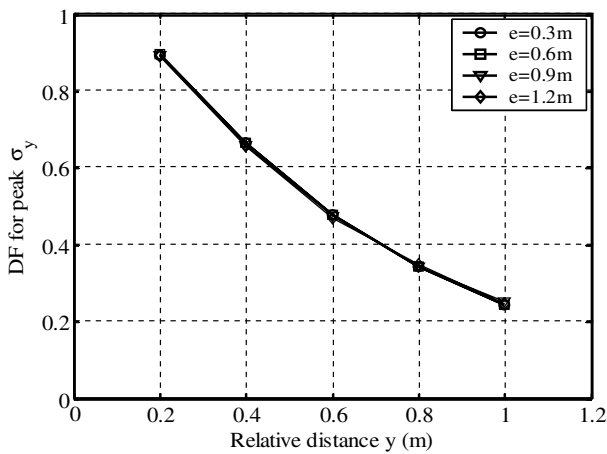


Fig. 7. Variation of decay factors for peak σ_y with different positions e of cavity.

$e = 0.6$ m and $h = 0.3$ m. Fig. 11 shows the effect of different lengths l on the attenuation of the peak σ_y . The results show that the peak σ_y increases with relative distance y and decreases with increasing length l . The corresponding relationship between DF for the peak σ_y and relative distance y is shown in Fig. 12. It can be established that DF decreases with increasing y and increases with cavity length for the same y .

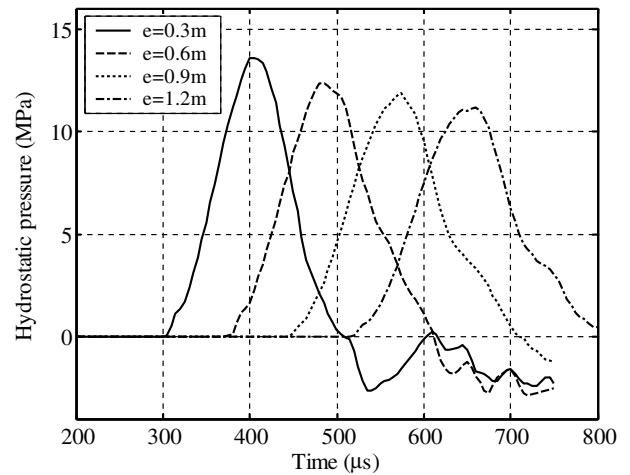


Fig. 8. Effect of cavity position e on hydrostatic pressure history at $y = 0.5$ m point on Y-axis.

4.2.2. Effect of cavity width h

Four values of $h = 0.3, 0.6, 0.9, 1.2$ m when $l = e = 0.3$ m are considered to study the effect of cavity width on the attenuation of stress-waves. The numerical results are shown in Fig. 13. It is noted that the cavity width h has little influence on the decay factor for the peak σ_y . Fig. 14 shows the damage contours for $h = 0.60$ m at a time of $524 \mu\text{s}$, which indicates that

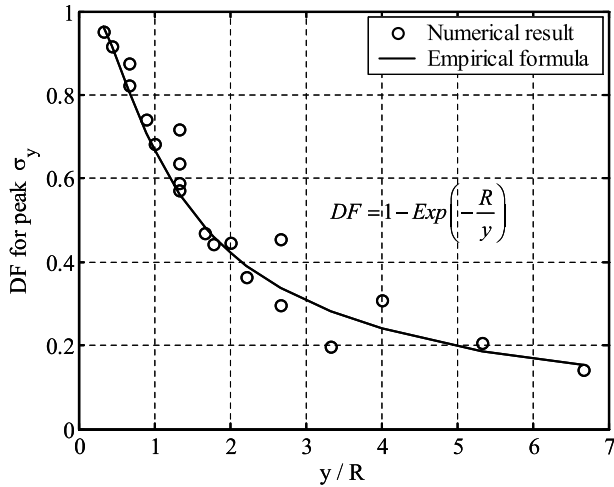


Fig. 9. Comparison of empirical formulae and numerical results of decay factors for the peak σ_y .

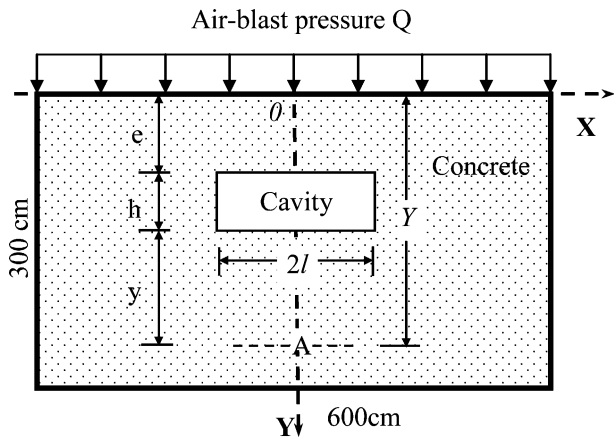


Fig. 10. Computational domain and dimensions for rectangular cavity scheme.

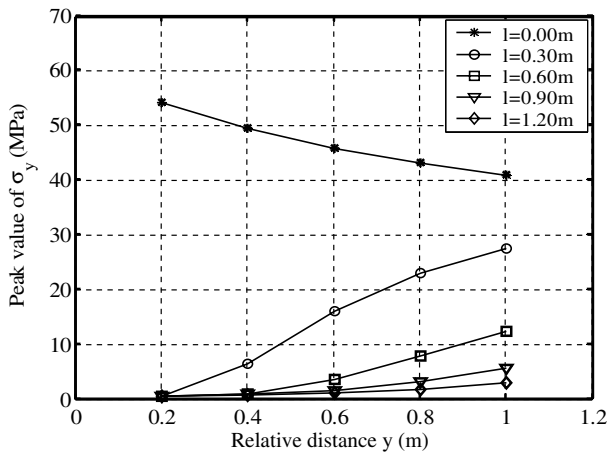


Fig. 11. Variation of the peak σ_y with different lengths l of cavity.

the high damage zone is located only near the upper surface and approaches zero at the zone beneath the cavity.

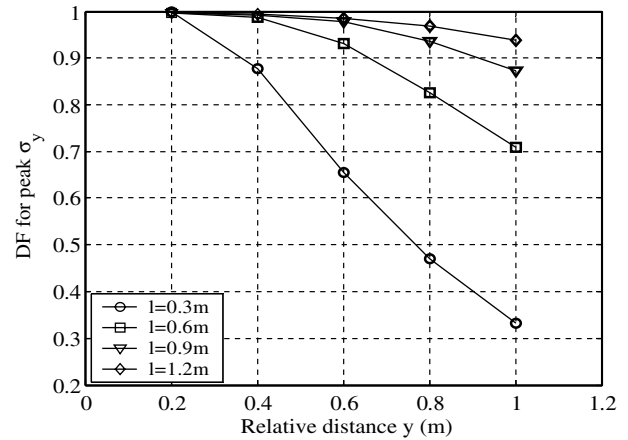


Fig. 12. Variation of decay factors for the peak σ_y with different lengths l of cavity.

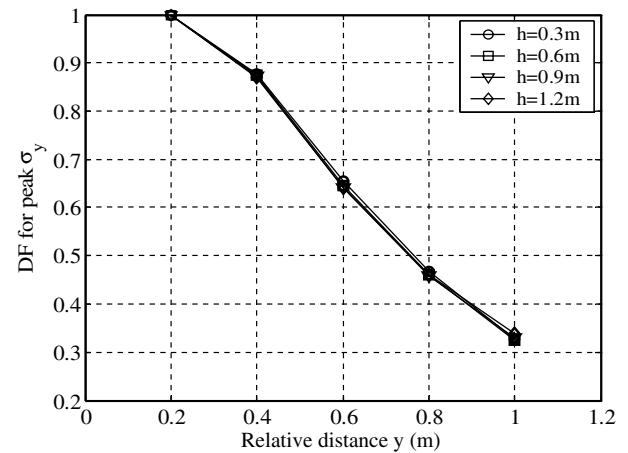


Fig. 13. Variation of decay factors for peak σ_y with different widths h of cavity.

4.2.3. Effect of cavity position e

The effect of cavity position e is examined here. The e values are taken as 0.3, 0.6, 0.9 and 1.2 m and $l = h = 0.3$ m. Fig. 15 shows the decay factor of the peak σ_y versus relative distance y . It is evident that all the curves are practically identical. Therefore, the position e of the cavity has little influence on the decay factor for the peak σ_y , similar to the case of circular cavity presented earlier. Fig. 16 compares the curves of σ_y versus t . For all e values, the peak values do not vary much, but the arrival time of the peak values gradually lags with an increase of the propagation distance of stress-waves.

4.2.4. Empirical formula for decay factor

Based on the above numerical results, the effects of h and e on the peak σ_y are established to be insignificant. Thus, DF is only a function of length l and relative distance y

$$DF = f(l, y) \quad (12)$$

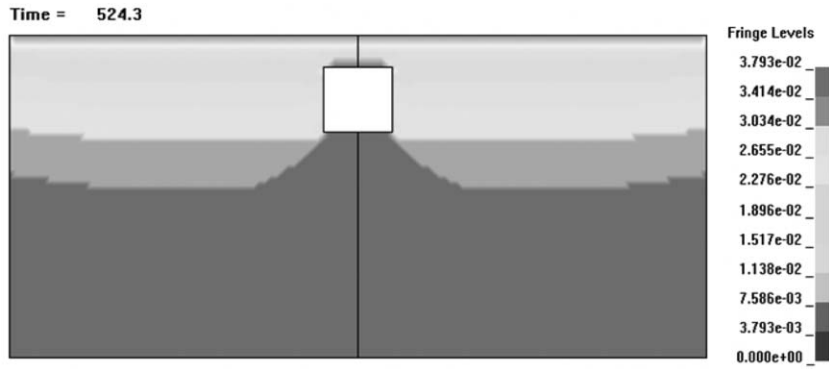


Fig. 14. Damage distribution for the $h = 0.60$ m ($e = l = 0.30$ m) case at $t = 524$ μ s.

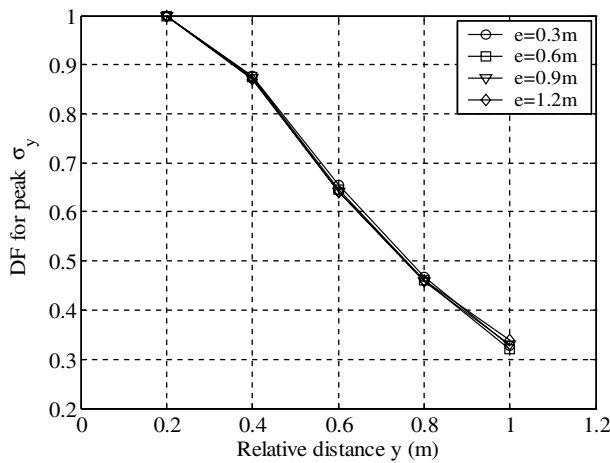


Fig. 15. Variation of the decay factors for peak σ_y with different positions e of cavity.

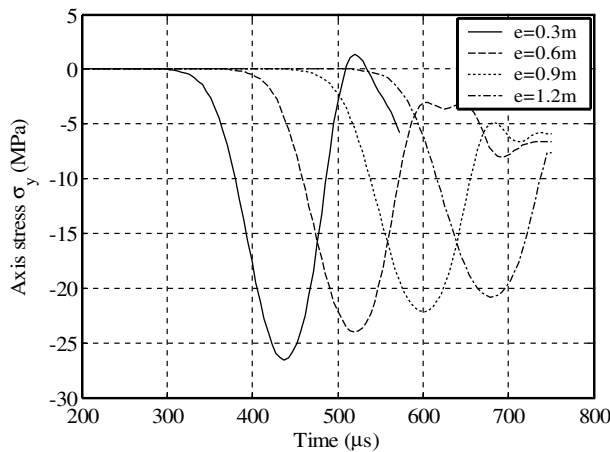


Fig. 16. Effect of cavity position e on σ_y history at $y = 0.8$ m point on Y -axis.

Based on the results shown in Fig. 12, one value of h (0.3 m), four values of l (0.3, 0.6, 0.9 and 1.2 m) and five values of y (0.2, 0.4, 0.6, 0.8 and 1.0 m) are chosen in the computations to obtain the following regression curve for the peak σ_y at the points just beneath the cavity

$$DF = \exp \left[- \left(\frac{y}{3l} \right)^2 \right] \quad (13)$$

This empirical formula shows that DF increases with l but decreases with increasing y . DF is equal to unity when $\frac{y}{l}$ approaches 0. Fig. 17 shows a comparison between the numerical results and the predictions from the empirical formula. This empirical formula is in good agreement with the numerical results. Therefore, Eq. (13) can be used to estimate the length l (or the whole length $2l$) of a rectangular cavity if the expected DF at a relative distance y is given. When DF and l are given, Eq. (13) can be also used to estimate the nearest safe distance (i.e., y_{\min}).

In defense engineering, the DF value at a specified position beneath a cavity is required to ensure the safety of the underground structures. For this purpose, Eqs. (10) and (13) can be used to estimate the minimum radius (R_{\min}) or length (l_{\min}) of a cavity. For example, when $y = 1.0$ m and $DF \geq 0.5$, l_{\min} should be at least 0.40 m for a rectangular cavity while the radius R_{\min} should be at least 0.69 m for a circular cavity. The attenuation effect of a circular cavity is much lower than that of a rectangular cavity if $R = l$.

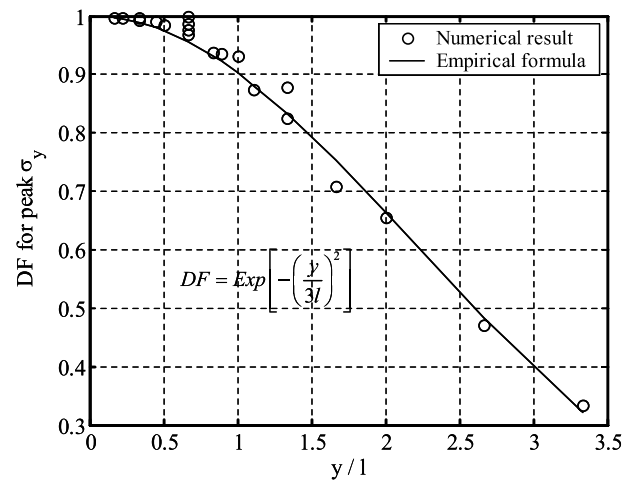


Fig. 17. Comparison of empirical formulae and numerical results of the decay factors for the peak σ_y .

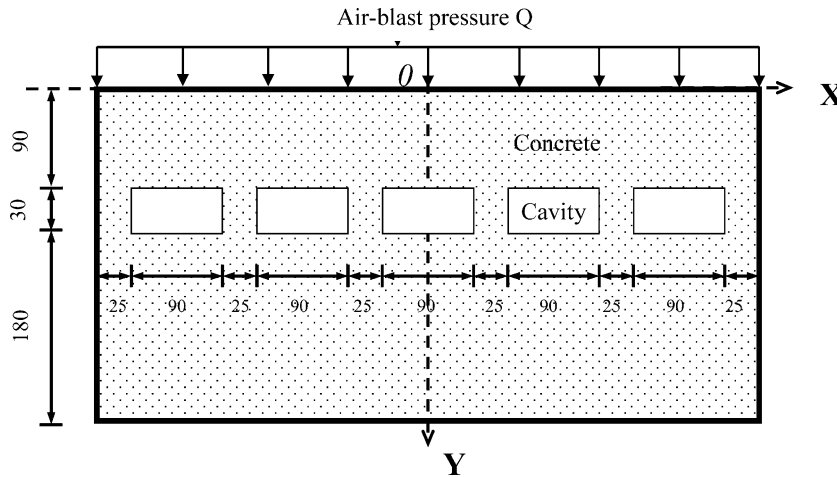


Fig. 18. Computational domain for multiple rectangular cavities scheme (unit: cm).

4.3. Effects of multiple cavities

The above results indicate that a single cavity exerts a great influence on the attenuation of stress-waves. In practice, a screen of multiple artificial cavities is usually formed to insulate and diffract stress-waves. Fig. 18 depicts a typ-

ical defense layer embedded with five rectangular cavities (0.9×0.3 m). The spacing between two neighborhood cavities for this case study is 0.25 m. The same triangular impulse loading shown in Fig. 2 is applied to the upper surface. The insulating effect between multiple cavities and a single cavity on the reduction of the peak σ_y when $e = 0.9$ m and $h = 0.3$ m is compared. Fig. 19(a) shows that the decay factor for the peak σ_y of multiple cavities is much higher than that of single cavity. However, when the relative distance is less than 1.0 m, the effect of multiple cavities ($l = 0.45$ m) is rather close to that of single cavity with $l = 0.60$ m. Fig. 19(b) compares the decay factor for the peak σ_y in the lateral direction at the points for $y = 1.0$ m. With the increase of lateral distance x , the peak σ_y of multiple cavities fluctuates around a stable value (i.e., 12.0 MPa). The peak value is also much lower than that of single cavity. Besides, one can see that the peak σ_y of single cavity is almost the same to the one without any cavity (i.e., 38.2 MPa) when $x > 1.2$ m. Apparently, the shielding effect is much better for multiple cavities than for a single cavity. A screen against stress-waves is formed through multiple cavities. This screen can effectively reduce the magnitude of stress-waves beneath the cavity.

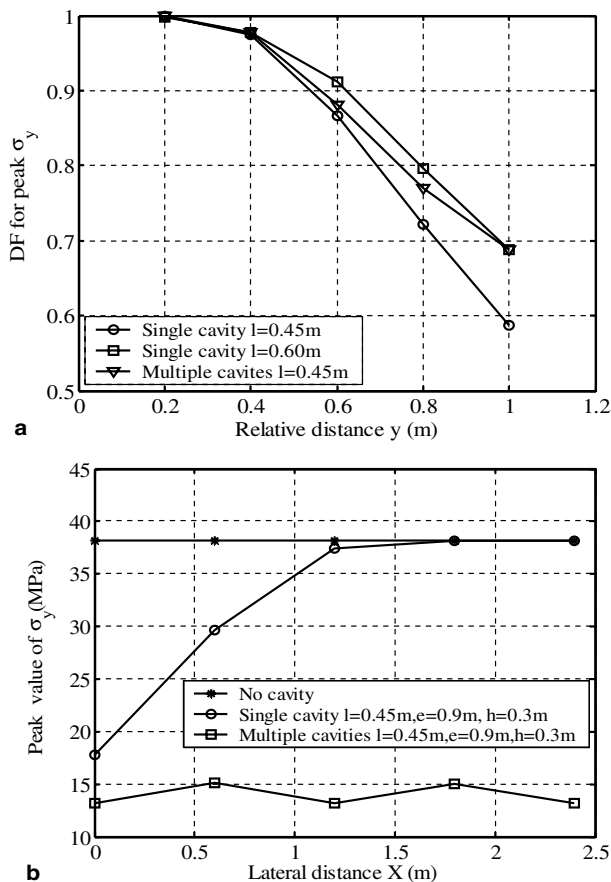


Fig. 19. Comparisons of screen effect between single and multiple rectangular cavities. (a) Curves of axial stress versus relative distance. (b) Curves of axial stress versus lateral distance.

5. Conclusions

The effects of circular and rectangular cavities in a concrete defense layer on the diffraction and attenuation of stress-waves are investigated using the J-H-C model. Two empirical formulae are proposed to describe the decay factor of the peak axial stress. In addition, the screen effect due to multiple rectangular cavities is analyzed. From these studies, the following conclusions and understandings can be drawn.

- (1) The elastoplastic and damage properties of concrete have great influence on the magnitude of axial stress σ_y in the concrete defense layer. The J-H-C model is

capable of evaluating the elastoplastic and damage effects of concrete on the reduction of the axial stress σ_y . Thus, the model can be employed for the design of concrete defense layer.

- (2) Cavities embedded in the concrete defense layer have a vital effect on the attenuation of stress-waves. For a circular cavity, the radius R has a significant effect on the reduction of stress-waves. For a rectangular cavity, the decay factor largely depends on its length, while its width has little effect if the width is larger than 0.3 m in our computations.
- (3) Empirical formulae are obtained to correlate the decay factor, dimensions of a cavity and relative distance. These formulae can be employed to determine the minimum length or radius of a cavity, or minimum safe distance y_{\min} when the decay factor is given. Therefore, these formulae can serve as useful tools in the design of intelligent defense layer in defense engineering.
- (4) Multiple cavities can form a screen to reduce the magnitude of stress-waves. The decay factor at any point beneath this screen is much higher than that of a single cavity. The shielding effect is also pronounced especially in the transverse direction.

It should be noted that the above conclusions are applicable only when the damage of concrete does not initiate the collapse of the cavity. Further work is necessary when the damage of concrete defense layer is severe enough to cause a complete collapse of the cavity.

Acknowledgement

This work reported herein was partially supported by the Post-doctoral Science Foundation of China (Project No. 2004036468).

References

- [1] Dowding CH. Construction vibrations. Upper Saddle River, NJ: Prentice Hall; 1996.
- [2] Yang Z. Finite element simulation of response of buried shelters to blast loadings. *Finite Elem Anal Design* 1997;24(3):113–32.
- [3] Achenbach JD. Wave propagation in elastic solids. Amsterdam: North-Holland; 1973.
- [4] Bostrom A, Grahn T, Niklasson AJ. Scattering of elastic waves by a rectangular crack in an anisotropic half-space. *Wave Motion* 2003;38:91–107.
- [5] Rohani B. Shielding methodology for conventional kinetic energy weapons. Technical report SL-8f-8. US army engineers corps, waterways experimental station, Vicksburg. M.S.; 1987, p. 43–56.
- [6] Philippidis TP, Aggelis TG. Experimental study of wave dispersion and attenuation in concrete. *Ultrasonics* 2005;43(7):584–95.
- [7] Balandin DY, Bolotnik NN, Pilkey WD. Optimal protection from impact, shock, and vibration. Gordon and Breach Science Publishers; 2001.
- [8] Li YC, Wang XJ, Hu XZ. Study on layered design and its defending function. Technical report of national defense engineering, USTC, China, 2004, p. 1–55.
- [9] Kenedey RP. A review of procedure for the analysis and design of concrete structure to resisting missile impact effects. *Nucl Eng* 1976;37(2):183–203.
- [10] Langheim H, Pahl H, Schmolinske E, Alois S. Subscale penetration tests with bomb-advanced penetration against hardened structures. In: Proceedings of the 6th international symposium on interaction of non-nuclear munitions with structures, Panama; 1993, p. 166–83.
- [11] Stearn SM. The concentration of dynamic stress in a plate at a sharp change of section. *J Sound Vib* 1971;15:353–67.
- [12] Liu DK, Liu HW. Scattering and dynamic stress concentration of SH wave by inter-surface circular hole. *Acta Mech Sinica* 1998;30(5):597–604.
- [13] Wang ZL, Li YC, Wang JG. Study of stress waves in geomechanics and effect of a soil cover layer on wave attenuation using a 1D finite-difference method. *Comput Geosci* 2006; in press.
- [14] Peng SZ. Dynamic stress concentration in a ribbed plate using the acoustical wave propagator technique. *J Sound Vib* 2005;279:75–88.
- [15] Robinson DN. A displacement bound principle for elastic-plastic structures subjected to blast loading. *J Mech Phys Solids* 1970;18(1):65–80.
- [16] Dancygier AN, Yankelevsky DZ, Baum H. Behavior of reinforced concrete walls with internal plaster coating under exterior hard projectile impact. *ACI Mater J* 1999;91(1):116–25.
- [17] Holmquist TJ, Johnson GR, Cook WH. A computational constitutive model for concrete subjected to large strains, high strain rates, and high pressures. In: Proceedings of the 14th international symposium on ballistics (Que., Canada) 1993, p. 591–600.
- [18] Johnson GR, Holmquist TJ. A computational constitutive model for brittle materials subjected to large strains, high strain rates and high pressures. In: Meyers MA, Murr LE, Staudhammer KP, editors. Shock-wave and high strain-rate phenomena in materials. New York: Marcel-Dekker; 1992. p. 1075–82.
- [19] Baker WE. Explosion in air. Austin: University of Texas Press; 1973.
- [20] Kinney GF, Graham KJ. Explosive shocks in air. New York: Springer; 1985.
- [21] Guruprasad S, Mukherjee A. Layered sacrificial claddings under blast loading, part I-analytical studies. *Int J Impact Eng* 2000;24(9):957–73.
- [22] Bulson PS. Explosive loading of engineering structures. E & FN Spon Press; 1997.
- [23] Charlie WA, Dowden NA, Villano EJ, Veyera GE, Doehring DO. Blast-induced stress wave propagation and attenuation: centrifuge model versus prototype tests. *Geotech Test J* 2005;28(2):207–16.
- [24] Livermore Software Technology Corporation (LSTC). LS-DYNA keyword user's manual (CA, USA) 2003.
- [25] Hallquist JO. LS-DYNA theoretical manual. (CA, USA): LSTC Press; 1998.
- [26] Camborde F, Mariotti C, Donze FV. Numerical study of rock and concrete behaviour by discrete element modeling. *Comput Geotech* 2000;27:225–47.